RESEARCH PAPER

PCCP
www.rsc.org/pccp

Dissociation of acetone radical cation ($CH_3COCH_3^{+\bullet} \rightarrow CH_3CO^+ + CH_3^\bullet$): An *ab initio* direct classical trajectory study†

Smriti Anand and H. Bernhard Schlegel*

Department of Chemistry and Institute for Scientific Computing, Wayne State University, Detroit, 48202, MI, USA

Received 22nd July 2004, Accepted 23rd August 2004
First published as an Advance Article on the web 7th September 2004

The dissociation of acetone radical cation ($CH_3COCH_3^{+\bullet} \rightarrow CH_3CO^+ + CH_3^\bullet$) has been studied by *ab initio* direct classical trajectory calculations at the MP2/6-31G(d) level of theory. A total of 247 trajectories were initiated at the transition state of the keto–enol tautomerization. A microcanonical ensemble using quasiclassical normal mode sampling was constructed by distributing 10 kcal mol^{-1} of excess energy above the barrier. The dissociation is found to favor the loss of the newly formed methyl group in agreement with experiments. The branching ratio of methyl loss was calculated to be 1.53 ± 0.20 which is fortuitously in very good agreement with the experimental ratio of 1.55 for 8–12 kcal mol^{-1} excess energy. Nearly 50% of the available energy is retained by the acetyl fragment as vibrational energy. The methyl fragment has very little vibrational energy but receives *ca*. 25% of the available energy in translation. The translational energy distribution of the methyl radicals is bimodal with the newly formed methyl having higher average translational energy than that the methyl derived from the spectator group.

Introduction

For over 30 years, the dissociation of acetone radical cation has been the subject of many experimental and theoretical studies. This system is of renewed interest because of the complexity of the dissociation dynamics and the non-statistical nature of the dissociation. Recently, McAdoo has reviewed the gas phase chemistry of $C_3H_6O^{+\bullet}$ ions.[1] Of the various isomers, the enol and keto forms of acetyl cation have been of particular interest, with the enol form being more stable of the two.[2] The enol form can be generated readily from higher aliphatic ketones *via* the McLafferty rearrangement (by dissociative ionization *via* γ hydrogen transfer) or by cycloreversion of 1-methylcyclobutanol (Scheme 1).[3]

It is well known that the enol form of the acetone cation can isomerize to the keto form and dissociate to produce acetyl cation and methyl radical, with the dissociation favoring the loss of the newly formed methyl group (Scheme 2).[3,20]

Experiments give an average branching ratio of 1.4 : 1 for the loss of the active methyl *versus* loss of the spectator methyl.[9,11,15,17] This is inconsistent with RRKM theory, and it was proposed that the reaction proceeds with incomplete randomization of the internal energy before the dissociation.[3,5,6,8,9] Hence the dissociation is characterized by non-ergodic behavior with unimolecular dissociation occurring faster than intramolecular vibrational energy redistribution (IVR). Studies have also found that the methyl groups show a bimodal distribution with the newly formed methyl possessing a higher average translational energy.[4,6] The lower energy methyl resulted from fragmentation after the energy had been redistributed in the keto isomer.[6] Non-ergodic behavior in the dissociation of other $C_3H_6O^{+\bullet}$ isomers (in particular, methyl vinyl ether and propene oxide) has also been observed.[21,22]

Osterheld and Brauman[17] studied the infrared multi-photon dissociation (IRMPD) of the acetone enol radical cation and confirmed that the two methyl groups are lost at an unequal rate. This non-statistical loss was found to increase with increasing internal energy above the dissociation threshold. The branching ratio of 1.16 at 0–3 kcal mol^{-1} above the barrier increased to 1.55 at 8–12 kcal mol^{-1} energy above the barrier. The implication is that a mode (other than the reaction coordinate) in the transition state of the keto–enol isomerization affects the non-statistical dissociation. The C–C–O bending mode involving the spectator methyl group was thought to be a strong candidate for affecting the non-statistical behavior.

Heinrich *et al.*[10] have used RRKM studies on an *ab initio* potential energy surface (PES) to study two competing reactions (methyl loss and methane elimination, Scheme 3) of the acetone radical cation. They proposed that the formation of an intermediate ion-molecule complex ($CH_3CO^+ \cdots CH_3^\bullet$) is common to both the reaction channels. This complex was calculated to be only *ca*. 16 kcal mol^{-1} above the keto isomer and 5 kcal mol^{-1} below the dissociated products. Bertran and co-workers[23] have carried out *ab initio* calculations at the

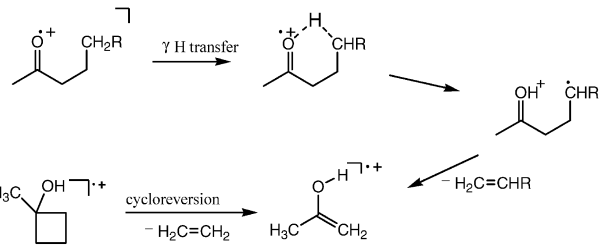

Scheme 1

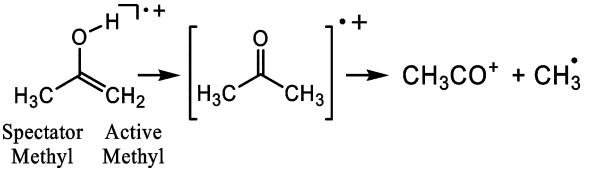

Scheme 2

† Electronic supplementary information (ESI) available: Calculated geometries for species **1, 2, 3, 4, TS1, TS2 and TS3** at all levels studied. See http://www.rsc.org/suppdata/cp/b4/b411229f/

DOI: 10.1039/b411229f

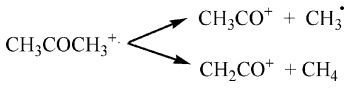

Scheme 3

MP3/6-311G(d,p) level of theory to study the ground state potential energy surface (PES) of acetone radical cation. Both these studies showed that methyl loss was the dominant channel at higher internal energies and the methane elimination channel is dominant at low internal energies of the reactant ion. Based on the calculated PES, hydrogen atom tunneling was thought to be an important factor in the methane elimination channel. However, Osterheld and Brauman[16] have carried out IRMPD studies on deuterated acetone cation and found that the methane loss does not involve tunneling. According to their experimental studies, the barrier to the H atom transfer (resulting in methane elimination) lies below the threshold for methyl loss and that this transfer does not require tunneling through a barrier. The large isotope effect observed by them was attributed to competition between the methane and methyl loss channels. However, the disparity between theory and experiment concerning the role of tunneling in methane elimination is a point that needs to be clarified.

Nummela and Carpenter[19] have used classical trajectory calculations to look at the non-statistical methyl loss from acetone radical cation. Direct dynamics calculations were carried out with the AM1-SRP method, employing specific reaction parameters fitted to density functional theory (DFT) calculations at the B3LYP/cc-pVTZ level of theory. When the trajectories were initiated at the transition state for the keto–enol isomerization, the branching ratio for the active methyl to the spectator methyl was calculated to be 1.13. However, trajectories started in the vicinity of the keto isomer gave a branching ratio of 1.01 and showed a statistical behavior in the dissociation.

Mintz and Baer[24] used photoion–photoelectron coincidence (PEPICO) spectroscopy to study the kinetic energy release distribution (KERD) of both the acetyl and methyl fragments in the dissociation of energy selected acetone ions. Another PEPICO study by Powis and Danby[25] showed that the KERD peaks for the acetyl ion fragment are broad and the mean kinetic energy release increases with increasing excess energy of the parent ion. Both these studies found a larger translational energy release for the methyl fragment than that predicted by quasi-equilibrium theory.

Majumdar *et al.*[26] have studied the multi-photon ionization (MPI) of acetone at 355 nm using time-of-flight mass spectrometry. They suggested that the parent ion could continue absorbing photons (ladder climbing) or it could dissociate into CH_3CO and CH_3 fragments which could absorb photons (ladder switching). The translational energy of the acetyl cation showed a linear increase with laser intensity. They found that at low to medium intensity of the laser, no ladder switching is observed but that at higher laser intensities, this mechanism does contribute. Futrell and co-workers[27, 31] have studied the collision induced dissociation (CID) of the enol form of acetone radical cation at energies up to 41 eV. These studies have lead to the conclusion that electronic excitation plays an important role in the dissociation dynamics. The large kinetic energy release in the products results from the fast and efficient conversion of the electronic energy to translational energy.

In the present paper, we use *ab initio* direct classical trajectory calculations to study the dissociation of acetone radical cation. Information about the PES is obtained 'on the fly' from electronic structure theory calculations without fitting to an analytical form.[32] A previous study[19] used semi-empirical calculations with parameters adjusted to fit density functional calculations. The current work employs high level *ab initio* molecular orbital calculations to compute accurate energetics for the dissociation reactions and *ab initio* molecular dynamics at the MP2/6-31G(d) level of theory to study the branching ratio and product energy distributions.

Method

The Gaussian[33] suite of programs was used to carry out the *ab initio* electronic structure and molecular dynamics calculations. The geometries of the minima and the transition states were computed at the Hartree–Fock (HF), Becke's three parameter hybrid density functional method[34, 36] (B3LYP), second order Møller–Plesset perturbation theory (MP2) and the quadratic configuration interaction with single and double excitations (QCISD).[37] The complete basis set extrapolation methods (CBS-QB3 and CBS-APNO) of Petersson and coworkers[38] were used to compute accurate energy differences. The CBS-APNO calculations have a mean absolute deviation of 0.5 kcal mol^{-1} for heats of reaction.

Ab initio classical trajectories were computed at the MP2/6-31G(d) level of theory using a Hessian based predictor-corrector method.[39,40] A predictor step is taken on the quadratic surface obtained from the energy, gradient and Hessian from the beginning point. A fifth order polynomial is then fitted to the energies, gradients and Hessians at the beginning and end points of the predictor step and a corrector step is taken on this fitted surface using the Bulirsch–Stoer algorithm.[41] The Hessians are updated for five steps before being recalculated analytically. The trajectories were terminated when the centers of mass of the fragments were 10 a_0 apart and the gradient between the fragments was less than 1×10^{-5} $E_h\ a_0^{-1}$. A step size of 0.5 $u^{1/2}\ a_0$ was used for integrating the trajectories. The energy was conserved to better than 1×10^{-6} E_h and the angular momentum was conserved to 1×10^{-8} $\hbar$.

Trajectories were initiated at the transition state for the keto–enol tautomerization. A microcannonical ensemble of initial states was constructed using the quasi-classical normal mode sampling.[42,43] A total energy of 10 kcal mol^{-1} above the zero point energy of the transition state was distributed among the 23 vibrational modes and translation along the transition vector. The total angular momentum was set to zero corresponding to a rotationally cold distribution and the phases of the vibrational modes were chosen randomly. For each initial condition, the momentum and displacement were scaled so that the desired total energy was the sum of the vibrational kinetic energy and the potential energy obtained from the *ab initio* surface. The initial conditions are similar to those chosen by Nummela and Carpenter.[19] A total of 250 trajectories were integrated. Of these, three trajectories were discarded because the anharmonicity of the PES resulted in improper scaling of the momentum and displacement.

Results and discussion

Structures and energetics

The key equilibrium structures and transition states on the potential energy surface for acetone radical cation isomerization and dissociation are collected in Fig. 1. The geometric parameters optimized at the QCISD/6-311G(d,p) level of theory are also shown in the Figure (details of the geometries at this and other levels of theory can be found in the supplementary material). There is good agreement with previous calculations at lower levels of theory.[10,23] The keto form of acetone radical cation, **2**, belongs to the C_2 point group and the methyls are rotated about 9–10° with respect to the C–O bond as noted in an earlier study.[10] However, the structure with C_{2v} symmetry (with the methyl groups eclipsed to the C–O bond) is only about 0.01 kcal mol^{-1} higher in energy than the C_2 structure and shows one small imaginary frequency corresponding to rotation of the methyl groups. The structure with both the methyl groups staggered (C_s symmetry) is 0.3–0.6 kcal

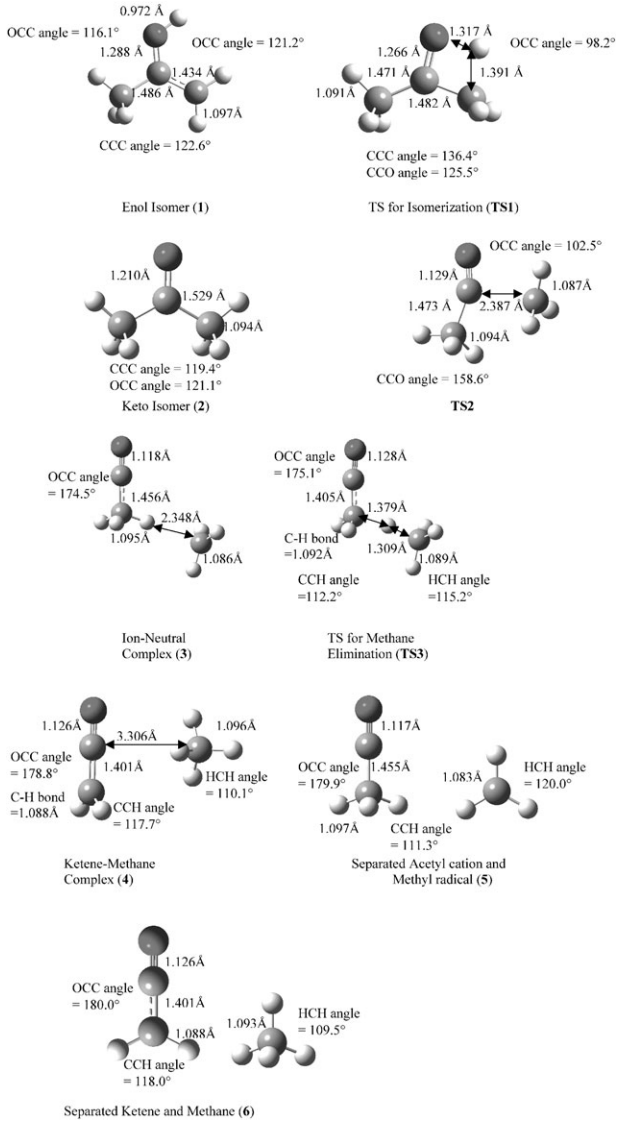

Fig. 1 Structures and selected geometric parameters of stationary points on the acetone radical cation potential energy surface optimized at the QCISD/6-311G(d,p) level of theory

mol^{-1} higher in energy than the C_{2v} structure and has a similar mode with an imaginary frequency. Thus, the methyl groups behave as free rotors. The enol form of acetone radical cation, **1**, has a delocalized π system involving the oxygen and the C–C double bond and is of A″ symmetry. The C–O bond length is only 0.03–0.07 Å longer than in keto isomer and the C–C bond is 0.07–0.10 Å shorter. The path to the keto–enol isomerization transition state involves a 90° rotation of the methylene group to yield a structure with C_s symmetry and an A′ electronic state which is about 10 kcal mol^{-1} higher than the A″ minimum. In the isomerization transition state, **TS1**, the O–H distance is about 40% longer than the O–H bond in the enol isomer, and the C–H distance is about 35% longer than the C–H bond in the keto isomer. The imaginary frequency in **TS1**, 1953 cm^{-1} at the MP2/6-31G(d) level of theory, corresponds to the migration of a hydrogen from the oxygen to the methylene carbon. This carbon atom makes an angle of about 98° with the C–O bond; however, the other CCO angle has not increased substantially. Proceeding from **TS1**, the A′ symmetry is retained throughout the H transfer and the methyl dissociation.

The keto isomer, **2**, dissociates to an ion–molecule complex between the acetyl cation and the methyl radical, **3**. At lower levels of theory, a transition state, **TS2**, can be found between **2** and **3**, but the reverse barrier may disappear at higher levels of theory.[23] The methyl radical in **3** is positioned ideally to abstract a hydrogen from acetyl cation to form ketene cation and methane. In this transition state, **TS3**, the hydrogen is situated midway between the two carbons and the C–C distance is 0.7–0.9 Å shorter than in complex **3**. Ketene cation and methane form a complex, **4**, before dissociating to products, **6**.

Table 1 lists the heats of the reaction and barrier heights for isomerization, methyl loss and methane elimination. The energy profiles for selected levels of theory are shown in Fig. 2. As seen from Table 1, the HF level predicts the barrier for keto–enol isomerization to be about 20–25 kcal mol^{-1} too high whereas DFT and all post-SCF level methods give barrier heights in good agreement with the experimental value and the CBS-APNO calculations. The enol isomer of acetone radical cation, **1**, is found to be lower in energy than the keto isomer, **2**. This is opposite to what is observed in the neutral species.[44,45] For the energy difference between **1** and **2**, the agreement with experiment and high level calculations is better with MP2 and large basis set DFT calculations than for HF and small basis DFT calculations.

As seen from the energy profile in Fig. 2, dissociation proceeds through the ion molecule complex **3**. The reverse barrier (**3** → **2**) is small and may disappear entirely at higher levels of theory. From **3**, loss of methyl radical is endothermic by *ca.* 5 kcal mol^{-1}. The methyl radical in **3** can also abstract a hydrogen atom *via* **TS3** resulting in the formation of ketene cation and methane. Earlier calculations placed **TS3** *ca.* 3 kcal mol^{-1} above the products for methane and methyl loss.[10] Thus, tunneling had to be invoked to explain the observation that methane loss dominates at low energies. However, subsequent experiments showed that tunneling was not important.[16] The more accurate CBS-QB3 and CBS-APNO calculations in the present work resolve this paradox. The energy of the transition state for methane elimination is lower than the energy of the methane + ketene cation product, and both are lower in energy

Table 1 Energies of the various points on the acetone radical cation PES[a]

	1	TS1	2	TS2	3	TS3	4	5	6
HF/3-21G	−1.8	59.0	0.0	24.2	21.6	34.9	23.3	24.6	24.2
HF/6-31G(d)	−3.0	55.9	0.0	24.3	20.3	36.5	21.6	22.4	22.1
B3LYP/3-21G	−3.8	38.8	0.0	—	17.4	16.2	16.4	27.6	23.4
B3LYP/6-31G(d)	−4.2	37.9	0.0	21.5	20.8	20.1	19.9	28.2	24.0
B3LYP/cc-pVTZ[b]	−10.2	38.1	0.0	—	—	—	—	24.4	—
MP2/6-31G(d)	−11.9	36.1	0.0	7.1	6.5	13.3	11.1	10.4	12.8
MP2/6-311+G(d,p)	−13.6	34.1	0.0	5.3	3.7	9.4	7.9	7.5	10.7
MP3/6-31G(d,p)[c]	−12.0	39.4	0.0	16.1	16.1	24.0	16.8	21.0	20.6
CBS-QB3	−7.6	35.8	0.0	—	17.6	19.6	16.9	21.1	20.1
CBS-APNO	−8.8	34.7	0.0	14.8	15.7	18.4	16.7	20.6	19.6
Experiment[d]	−13.8	37–45	0.0	—	—	—	—	20.1	20.5

[a] In kcal mol^{-1} at 298 K, relative to **2** (keto isomer). [b] Ref. 19. [c] Ref 10. [d] Refs 17, 47 and 48.

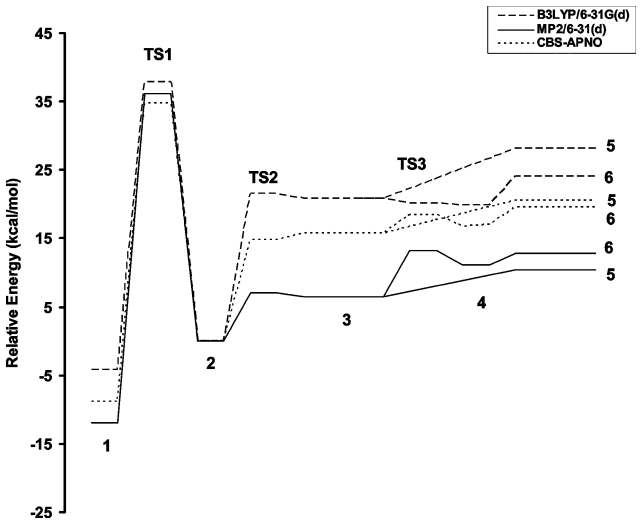

Fig. 2 Potential energy profile for the isomerization and dissociation of the acetone radical cation computed at the B3LYP/6-31G(d), MP2/6-31G(d) and CBS-APNO levels of theory

than the methyl radical + acetyl cation product. Thus at low energies, ketene cation + methane is preferred without the need to invoke tunneling. However, the methyl radical channel is only 1 kcal mol^{-1} higher in energy and does not involve a tight transition state. Thus acetyl cation and methyl radical will be the dominant product at higher temperatures.

Dynamics

Comparing the Hartree–Fock calculations to the high level calculations, the energy release from **TS1** to products is too large and the energy of **TS3** relative to products is too high. On the other hand, B3LYP calculations place the methyl radical + acetyl cation products, **5**, too high relative to methane + ketene cation, **6**. Thus, the Hartree–Fock and B3LYP calculations are probably not suitable for *ab initio* molecular dynamics calculations on this system. The MP2/6-31G(d) level of theory was chosen to integrate the trajectories because the relative energies for the methane channel (**TS3**, **4**, and **6**) compared to the methyl products, **5**, are in reasonable agreement with the CBS-APNO calculations while still being affordable for the dynamics. However, it should be kept in mind that the energy release on going from the transition state for keto–enol isomerization, **TS1**, to acetyl cation + methyl radical products, **5**, is 10 kcal mol^{-1} greater than computed at the CBS-APNO level of theory.

Of the 247 trajectories which were integrated, 130 resulted in the loss of the active methyl and 75 finished with the loss of the spectator methyl. Another 42 did not meet the stopping criteria in the 400 fs simulation time. Of these 42 trajectories, 28 would have met the stopping criteria if the simulation was run for an additional 50–100 fs or if the stopping criteria were made less stringent (separation between the fragments $\sim 8\ a_0$ and the gradient between the fragments was $1 \times 10^{-4}\ E_h\ a_0^{-1}$), with 11 trajectories losing the active methyl and 17 losing the spectator methyl. There were also 12 trajectories that went back to form the enol, **1**, and none remained in the keto minimum, **2**.

For most of the trajectories losing the active methyl, the dissociation takes place soon after the methyl group is formed and is completed in about 200 fs. For these trajectories, the formation of the methyl group, the linearization of the CCO angle and bond dissociation occur nearly concurrently, and the system spends very little time in the keto minimum, **2**, or the ion–molecule complex, **3**. This is in agreement with the observations of Nummela and Carpenter.[19] By contrast, all the trajectories that lost the spectator methyl did spend significant time in the keto minimum. After **2** is formed, the molecule

Table 2 Partitioning of the available energy[a]

	Translation	Rotation	Vibration	Total
Acetyl	3.6	2.51	18.74	24.85
Methyl	10.09	2.52	5.7[b]	13.69
Both	13.69	5.03	19.82	38.54
Percentages				
Acetyl (%)	9.3%	6.5%	48.6%	64.5%
Methyl (%)	26.2%	6.5%	2.8%	35.5%
Both (%)	35.5%	13.1%	51.4%	100.0%

[a] Energy in kcal mol^{-1}. [b] See text.

vibrates for a few tens of fs (corresponding to 1–2 vibrational cycles of the C–C stretch and CCO bend) before dissociating. However, this time is not sufficient for the re-distribution of the energy through all the vibrational modes (which is typically of the order of a few picoseconds[46]). Dissociation of the spectator methyl typically required about 300–380 fs, although a few trajectories finished in shorter times. Interestingly, there were about 30 trajectories which entered the PES minimum of **2** and lost the active methyl in about 250–360 fs. None of the trajectories resulted in the methane + ketene cation products even though there was more than sufficient energy available to overcome the barrier and form the products. The transition state for methane elimination, **TS3**, has a C–C distance that is 0.7–0.9 shorter than the ion-molecule complex, **3**. However, when complex **3** is formed from **TS1** under the present initial conditions, the methyl group has considerable translational energy and is more likely to continue to elongate the C–C distance toward dissociation rather than proceed through a tight transition state with a shorter C–C distance.

The partitioning of the available energy between the two fragments is summarized in Table 2. Overall, about 35% of the available energy goes into translation of both the fragments. This is in good agreement with the experimental value of 32%.[6] The methyl fragment receives about 10 kcal mol^{-1} in translation energy and about 4 kcal mol^{-1} goes into translation of the acetyl fragment. Rotation accounts for only about 13% of the available energy and is shared equally between the fragments. More than half of the available energy appears as vibrational energy of the fragments. The methyl radical is formed with very little vibrational energy. In about one quarter of the trajectories, the methyl fragments had less than 90% of zero point energy (ZPE). The acetyl cation is formed with an average of 19 kcal mol^{-1} of vibrational energy above ZPE, which corresponds to nearly 50% of the available energy. The acetyl cation is stable to dissociation, since its internal energy is much less than required for the lowest energy dissociation channel (CH_3^+ + CO, 77 kcal mol^{-1}). Most of the vibrational energy in the acetyl cation resides in the C–H stretches, the methyl umbrella motion and the CCO bending with very little energy in the C–C stretching mode.

Experimentally, the methyl fragments show a bimodal distribution in their translational energy.[4,5,46] The calculated translational energy distribution is plotted in Fig. 3. Although there is considerable overlap between the two sets of histograms, the active methyls have a larger average translational energy (11.4 kcal mol^{-1}) than the spectator methyls (7.8 kcal mol^{-1}).

The present calculations at the MP2/6-31G(d) level of theory yield a ratio of 1.73 ± 0.25 (130/75) for dissociation of the active methyl *vs.* the spectator methyl, in qualitative agreement with the experimental ratio of 1.55 at an excess energy of 8–10 kcal mol^{-1}.[17] If one includes the 28 incomplete trajectories that would have eventually dissociated, then 141 trajectories lose the active methyl and 92 lose the spectator methyl, yielding a branching ratio of 1.53 ± 0.20. However, the ratio is significantly higher if one excludes the trajectories in which

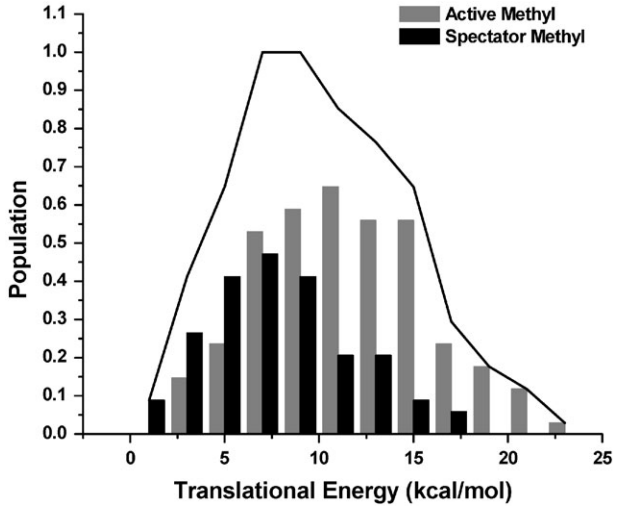

Fig. 3 Translational energy distribution of the methyl fragments derived from the active and spectator methyl fragments

the methyl fragments have less than ZPE. Nummela and Carpenter[19] obtained a significantly smaller ratio of 1.13 at the AM1-SRP level of theory. One possible explanation for the difference in the calculated branching ratios could be that the energy release at MP2/6-31G(d) is 10 kcal mol^{-1} greater than the CBS-APNO value, while in the AM1-SRP calculations of Nummela and Carpenter, the energy release is $\sim$4 kcal mol^{-1} too low.

Conclusions

The energetics of acetone radical cation dissociation has been studied by electronic structure calculations at various level of theory up to CBS-APNO. At the highest levels of theory, the transition state for methane elimination is lower in energy than the acetyl cation + methyl radical and ketene cation + methane products. Thus tunneling is not required to explain the observed kinetics. The non-statistical dissociation of acetone radical cation has been simulated by *ab initio* classical trajectories at the MP2/6-31G(d) level of theory starting from the transition state for keto–enol isomerization. The ratio of methyl radical production from the newly formed methyl to the existing methyl is calculated to be 1.53 $\pm$ 0.20 and is fortuitously in very good agreement with the experimental ratio of 1.55. However, higher levels of theory that gave a more accurate value for the energy release may alter this ratio. The acetyl cations formed carry *ca.* 50% of the available energy as internal energy. About 25% of the available energy ends up in methyl translational energy. The methyl fragment translational energies show a bimodal distribution with the newly formed methyl group having a larger average translational energy.

Acknowledgements

This work was supported by a grant from the National Science Foundation (CHE 0131157). Computer time made available by C&IT and ISC is gratefully acknowledged.

References

1 D. J. McAdoo, *Mass Spectrom. Rev.*, 2000, **19**, 38–61.
2 J. L. Holmes and F. P. Lossing, *J. Am. Chem. Soc.*, 1980, **102**, 1591–1595.
3 F. W. McLafferty, D. J. McAdoo, J. S. Smith and R. Kornfeld, *J. Am. Chem. Soc.*, 1971, **93**, 3720–3730.
4 C. Lifshitz, *Int. J. Mass Spectrom. Ion Phys.*, 1982, **43**, 179–193.
5 C. Lifshitz, P. Berger and E. Tzidony, *Chem. Phys. Lett.*, 1983, **95**, 109–113.
6 C. Lifshitz and E. Tzidony, *Int. J. Mass Spectrom. Ion Phys.*, 1981, **39**, 181–195.
7 C. Lifshitz and E. Tzidony, *Ann. Isr. Phys. Soc.*, 1981, **4**, 242–244.
8 C. Lifshitz, E. Tzidony, D. T. Terwilliger and C. E. Hudson, *Adv. Mass Spectrom.*, 1980, **8A**, 859–866.
9 G. Depke, C. Lifshitz, H. Schwarz and E. Tzidony, *Angew. Chem., Int. Ed. Engl.*, 1981, **20**, 792–793.
10 N. Heinrich, F. Louage, C. Lifshitz and H. Schwarz, *J. Am. Chem. Soc.*, 1988, **110**, 8183–8192.
11 D. J. McAdoo and C. E. Hudson, *Int. J. Mass Spectrom. Ion Processes*, 1984, **59**, 77–83.
12 D. J. McAdoo and C. E. Hudson, *Int. J. Mass Spectrom. Ion Processes*, 1984, **62**, 269–276.
13 D. J. McAdoo, F. W. McLafferty and J. S. Smith, *J. Am. Chem. Soc.*, 1970, **92**, 6343.
14 D. J. McAdoo and D. N. Witiak, *J. Chem. Soc., Perkin Trans. 2*, 1981, 770–773.
15 F. Turecek and V. Hanus, *Org. Mass Spectrom.*, 1984, **19** 631–638.
16 T. H. Osterheld and J. I. Brauman, *J. Am. Chem. Soc.*, 1992, **114**, 7158–7164.
17 T. H. Osterheld and J. I. Brauman, *J. Am. Chem. Soc.*, 1993, **115**, 10311–10316.
18 F. Turecek and F. W. McLafferty, *J. Am. Chem. Soc.*, 1984, **106**, 2525.
19 J. A. Nummela and B. K. Carpenter, *J. Am. Chem. Soc.*, 2002, **124**, 8512–8513.
20 R. C. Heyer and M. E. Russell, *Org. Mass Spectrom.*, 1981, **16**, 236–237.
21 F. Turecek and F. W. McLafferty, *J. Am. Chem. Soc.*, 1984, **106**, 2528.
22 C. Lifshitz, *Org. Mass Spectrom.*, 1988, **23**, 303–306.
23 M. D. Ceno, A. Gonzalez-Lafont, J. M. Lluch and J. Bertran, *Mol. Phys.*, 1997, **92**, 393–398.
24 D. M. Mintz and T. Baer, *Int. J. Mass Spectrom. Ion Phys.*, 1977, **25**, 39–45.
25 I. Powis and C. J. Danby, *Int. J. Mass Spectrom. Ion Phys.*, 1979, **32**, 27–33.
26 C. Majumder, O. D. Jayakumar, R. K. Vatsa, S. K. Kulshreshtha and J. P. Mittal, *Chem. Phys. Lett.*, 1999, **304**, 51–59.
27 K. Qian, A. Shukla and J. Futrell, *Chem. Phys. Lett.*, 1990, **175** 51–54.
28 K. Qian, A. Shukla and J. Futrell, *J. Chem. Phys.*, 1990, **92**, 5988–5996.
29 K. Qian, A. Shukla, S. Howard, S. Anderson and J. Futrell, *J. Phys. Chem.*, 1989, **93**, 3889–3892.
30 A. K. Shukla, K. Qian, S. L. Howard, S. G. Anderson, K. W. Sohlberg and J. H. Futrell, *Int. J. Mass Spectrom. Ion Processes*, 1989, **92**, 147–169.
31 R. Zhao, R. Tosh, A. Shukla and J. Futrell, *Int. J. Mass Spectrom. Ion Processes*, 1997, **167–168**, 317–333.
32 K. Bolton, W. L. Hase and G. H. Peslherbe, in *Modern Methods for Multidimensional Dynamics Computation in Chemistry*, ed. D. L. Thompson, World Scientific, Singapore, 1998, p. 143.
33 M. J. Frisch, G. W. Trucks, H. B. Schlegel, G. E. Scuseria, M. A. Robb, J. R. Cheeseman, J. A. Montgomery Jr., T. Vreven, K. N. Kudin, J. C. Burant, J. M. Millam, S. S. Iyengar, J. Tomasi, V. Barone, B. Mennucci, M. Cossi, G. Scalmani, N. Rega, G. A. Petersson, H. Nakatsuji, M. Hada, M. Ehara, K. Toyota, R. Fukuda, J. Hasegawa, M. Ishida, T. Nakajima, Y. Honda, O. Kitao, H. Nakai, M. Klene, X. Li, J. E. Knox, H. P. Hratchian, J. B. Cross, C. Adamo, J. Jaramillo, R. Gomperts, R. E. Stratmann, O. Yazyev, A. J. Austin, R. Cammi, C. Pomelli, J. W. Ochterski, P. Y. Ayala, K. Morokuma, G. A. Voth, P. Salvador, J. J. Dannenberg, V. G. Zakrzewski, S. Dapprich, A. D. Daniels, M. C. Strain, O. Farkas, D. K. Malick, A. D. Rabuck, K. Raghavachari, J. B. Foresman, J. V. Ortiz, Q. Cui, A. G. Baboul, S. Clifford, J. Cioslowski, B. B. Stefanov, G. Liu, A. Liashenko, P. Piskorz, I. Komaromi, R. L. Martin, D. J. Fox, T. Keith, M. A. Al-Laham, C. Y. Peng, A. Nanayakkara, M. Challacombe, P. M. W. Gill, B. Johnson, W. Chen and M. W. Wong, C. Gonzalez and J. A. Pople., *Gaussian Development Version (Revision C.01)*, Gaussian Inc., Wallingford, CT, 2004.
34 A. D. Becke, *J. Chem. Phys.*, 1993, **98**, 5648.
35 A. D. Becke, *J. Chem. Phys.*, 1993, **98**, 1372.
36 C. Lee, W. Yang and R. D. Parr, *Phys. Rev. B*, 1988, **37**, 785.
37 J. A. Pople, M. Head-Gordon and K. Raghavachari, *J. Chem. Phys.*, 1987, **87**, 5968.
38 J. A. Montgomery, J. W. Ochterski and G. A. Peterson, *J. Chem. Phys.*, 1994, **101**, 5900.

39 V. Bakken, J. M. Millam and H. B. Schlegel, *J. Chem. Phys*., 1999, **111**, 8773.
40 J. M. Millam, V. Bakken, W. Chen, W. L. Hase and H. B. Schlegel, *J. Chem. Phys*., 1999, **111**, 3800.
41 J. Stoer and R. Bulirsch, *Introduction to Numerical Analysis*, Springer-Verlag, New York, 1980.
42 W. L. Hase, in *Encyclopedia of Computational Chemistry*, ed. P. v. R. Schleyer, N. L. Allinger, T. Clark, J. Gasteiger, P.A. Kollman, H. F. Schaefer, III and P. R. Schreiner, Wiley, Chichester, 1998, pp. 402–407.
43 G. H. Peslherbe, H. Wang and W. L. Hase, *Adv. Chem. Phys*., 1999, **105**, 171–201.
44 J. L. Holmes and F. P. Lossing, *J. Am. Chem. Soc*., 1982, **104**, 2648–2649.
45 N. Heinrich, W. Koch, G. Frenking and H. Schwarz, *J. Am. Chem. Soc*., 1986, **108**, 593.
46 C. Lifshitz, *J. Phys. Chem*., 1983, **87**, 2304–2313.
47 F. Turecek and C. J. Cramer, *J. Am. Chem. Soc*., 1995, **117**, 12243–12253.
48 J. C. Traeger, *Int. J. Mass Spectrom*., 2001, **210–211**, 181.